Flexible and Printed Electronics

Printed zinc tin oxide diodes: from combustion synthesis to large-scale manufacturing

Flexible and Printed Electronics

OPEN ACCESS

RECEIVED
13 September 2021

REVISED
4 January 2022

ACCEPTED FOR PUBLICATION
14 January 2022

PUBLISHED
31 January 2022

PAPER

Printed zinc tin oxide diodes: from combustion synthesis to large-scale manufacturing

Emanuel Carlos[1,*], Rita Branquinho[1], Elina Jansson[2], Jaakko Leppäniemi[3,*], José Menezes[1], Rita Pereira[1], Jonas Deuermeier[1], Ari Alastalo[3], Kim Eiroma[3], Liisa Hakola[3], Elvira Fortunato[1] and Rodrigo Martins[1,*]

[1] CENIMAT/i3N Departamento de Ciência dos Materiais, Faculdade de Ciências e Tecnologia (FCT), Universidade NOVA de Lisboa (UNL), and CEMOP/UNINOVA, Caparica 2829-516, Portugal
[2] VTT Technical Research Centre of Finland Ltd, Kaitoväylä 1, FI-90570 Oulu, Finland
[3] VTT Technical Research Centre of Finland Ltd, Tietotie 3, FI-02150 Espoo, Finland
[*] Authors to whom any correspondence should be addressed.

E-mail: e.carlos@campus.fct.unl.pt, jaakko.leppaniemi@vtt.fi and rm@uninova.pt

Keywords: solution combustion synthesis, metal oxides, printed Schottky diodes, low temperature, roll-to-roll (R2R)

Supplementary material for this article is available online

Abstract

Printed metal oxide devices have been widely desired in flexible electronic applications to allow direct integration on foils and to reduce electronic waste and associated costs. Especially, semiconductor devices made from non-critical raw materials, such as Zn, Sn (and not, for example, In), have gained significant interest. Despite considerable progress in the field, the upscale requirements from lab to fab scale to produce these materials and devices remain a challenge. In this work, we report the importance of solution combustion synthesis (SCS) when compared with sol–gel in the production of zinc tin oxide (ZTO) thin films using a solvent (1-methoxypropanol) that has lower environmental impact than the widely used and toxic 2-methoxyethanol. To assure the compatibility with low-cost flexible substrates in high-throughput printing techniques, a low annealing temperature of 140 °C was achieved for these thin films by combining SCS and infrared annealing in a short processing time. These conditions allowed the transition from spin-coating (lab scale) to flexographic printing (fab scale) at a printing speed of 10 m min^{-1} in a roll-to-roll pilot line. The ZTO (1:1 Zn:Sn-ratio) diodes show a rectification ratio of 10^3, a low operation voltage ($\leqslant$3 V), promising reproducibility and low variability. The results provide the basis for further optimisation (device size, encapsulation) to meet the requirements of diodes in flexible electronics applications such as passive-matrix addressing, energy harvesting and rectification.

1. Introduction

Over the last decade, printed electronics has been highlighted as one of the most promising technologies to boost the internet of things applications (wearables, low-cost sensors, touch displays, smart packaging and security tags) that cannot be fulfilled by conventional electronics [1–3]. This new era of electronics could be realized by sustainable, additive, on-demand large-area manufacturing, where complex systems are constructed through layer-by-layer integration while, at the same time, the associated production costs are minimized through high-throughput roll-to-roll (R2R) printing [4]. In order to reach even higher performances while keeping the low cost, printed electronics can be combined with conventional, thinned silicon integrated circuits (ICs), also referred to hybrid electronics, for niche products [5]. However, to implement the visions of printed electronics, breakthroughs should be made in the design and printing of the most ubiquitous electronic components such as transistors, capacitors, resistors, diodes, and memories [6–10]. Among them, metal oxide (MO) diodes play a crucial role for example in voltage regulation and surge protection that are required for wireless power transmission technology and in near-field communication when applied in flexible radio frequency identification tags [8]. For this application, the diodes should have low turn-on voltage, high cut-off frequency, and low leakage

current. Besides that, this field demands inexpensive and large-scale manufacturing which fits perfectly with printed techniques. However, spin-coating is the most common solution-processing technique reported in the fabrication of diodes due to its simplicity and versatility [8, 11–13]. By combining this technique with adhesion lithography, high-performance ZnO diodes were achieved, reaching operation frequencies up to 100 GHz thus being able to compete with conventional electronics [14]. Nevertheless, the fabrication of these components is not readily scalable to high-throughput R2R environments and requires subtractive processes, which increase the devices' final cost and complexity. Printed MO diodes could surpass the scalability issues as no external processes are needed to pattern these materials in a reproducible way and the amount of production waste could be significantly reduced through additive manufacturing [15]. Diverse non-contact (inkjet, aerosol jet, and electrohydrodynamic (EHD) jet printing) and contact printing techniques (reverse-offset, flexographic, rotary screen, and gravure printing) can be used in printed electronics manufacturing. To meet the demands of high-throughput, R2R manufacturing is desirable [16–21]. Cho *et al* reported the first hybrid ZnO diodes fabricated by R2R gravure printing at a printing speed of 8 m min^{-1} and some years later implemented these in wireless sensor-signage tags for smart packaging [22, 23]. However, since then only a few reports have been published, where printing techniques are used to produce MO diodes (table S1 in the supporting information available online at stacks.iop.org/FPE/7/014005/mmedia). Flexographic and gravure printing can reach high throughput (up to 1000 m min^{-1}). Among these two, flexographic printing is less expensive due to the use of polymeric stamps [18, 24]. Besides the printability, other important aspects to consider are the annealing temperature required to form the MO semiconductors from the liquid precursor inks and the annealing duration required to achieve a sufficient quality MO films. Processing temperatures are usually high (>250 °C), which can harm flexible substrates with lower melting points and high thermal expansion [8]. Annealing times over 10 min are unpractical to realize in R2R environment without separate off-line heating systems. To decrease the thermal budget and the annealing time to form the oxide materials, different approaches such as solution combustion synthesis (SCS) (boosts the local temperature during annealing by releasing chemical energy) [25] and various post-processing methods (such as photonic annealing) have been implemented [26, 27]. The photonic annealing has two main methods, pulsed (flash lamp) and continuous (ultraviolet (UV) or infrared (IR) lamp), where the power intensity, pulse duration and the number of pulses can be changed [27–29]. Tailoring these parameters allows a reduction of the processing time (deliver thermal energy within μs to ms time range) and the final temperature to form the MO layers, thus being fundamental in the upscaling efforts from the lab scale to the R2R pilot lines [30–33]. When the films are exposed to photonic annealing, this leads to the cleavage of alkoxy groups into active metals and oxygen atoms which facilitates the metal–oxygen–metal (M–O–M) network formation through radical-mediated chemical reactions [9, 34]. Therefore, the thin films' densification is enhanced in a short processing time. Besides these, other aspects should be considered to allow MO semiconductor devices take the transition from the lab scale to the pilot scale R2R and even further towards systems used in the printing industry. Those include (a) the use of Earth-abundant materials (Zn and Sn favoured over rareness of In); (b) inks based on solvents with lower environmental impact (i.e. greener solvents like ethanol and water) instead of commonly used toxic solvents like 2-methoxyethanol (2-ME); (c) application of low-cost flexible substrates (polyethylene terephthalate (PET), polyethylene naphthalate (PEN) and cellulose) rather than glass or silicon; (d) processing under controlled ambient conditions (humidity, temperature and atmosphere) to allow reproducibility; and (e) performing surface treatments to assure a good adhesion between layers [24, 26]. Nevertheless, most of the literature reported on printed MO devices focuses on the use of printing techniques at the lab scale.

In this work, we optimized the synthesis to form zinc tin oxide (ZTO) in a greener solvent 1-methoxypropanol (1-MP) as compared to the currently most used solvent, 2-ME, which is highly toxic and thus limits the application of these inks at larger scale. Especially in R2R environments, where the amount of ink is considerable (>100 ml's) and exposure of process personnel to hazardous, volatile solvents is more difficult to control than in lab-scale research environments. Low-temperature-annealed ZTO diodes were first attained by spin-coating a ZTO ink assisted by SCS method with IR lamp annealing. Then, ZTO layers were fabricated using flexographic printing by adjusting the viscosity of the ZTO ink and printing speed. Finally, for the first time, we performed the upscaling from the lab scale to pilot R2R scale and demonstrated fully-printed ZTO diodes with a low thermal budget ($\leqslant$140 °C), as depicted in figure 1. The results achieved with the R2R processing were on par with the ones processed by spin-coating, thus proving the suitability, stability and uniformity of the chosen, up-scaled procedures. This accomplishment paves a way to a new era of printed MO diodes with enormous potential for low-cost flexible applications.

2. Results and discussion

The solvent selection of the MO precursor ink has been shown to play a crucial role in the formation of

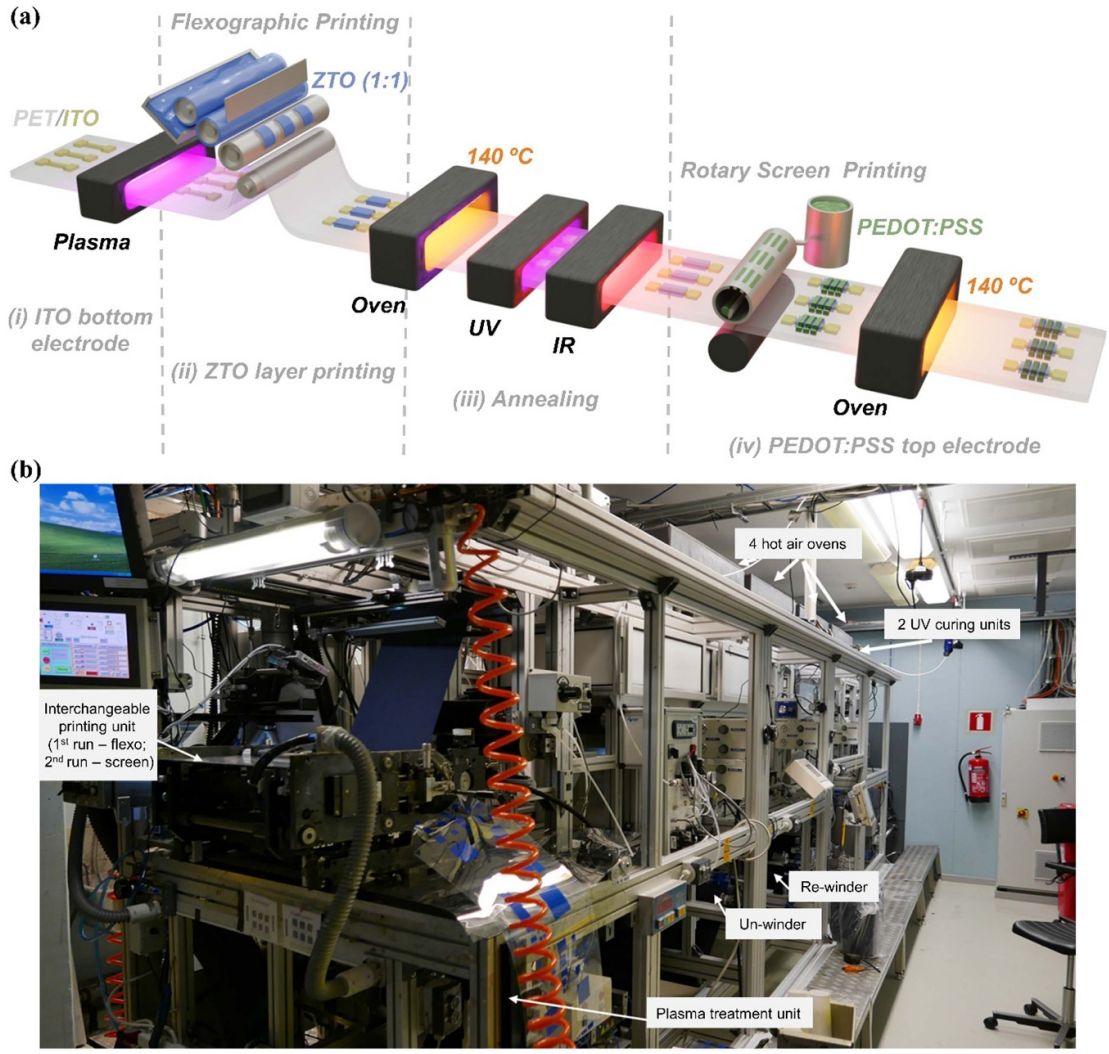

Figure 1. (a) Schematic representation of printing and annealing steps to produce the ZTO SCS diodes in the ROKO R2R-pilot line at VTT: (i) indium tin oxide (ITO) bottom electrode after R2R patterning by printing an etching paste; (ii) ZTO layer printing by flexography; (iii) annealing of the ZTO layer using in-line oven, UV and IR units; (iv) poly(3,4-ethylenedioxythiophene) polystyrene sulfonate (PEDOT:PSS) top-electrode fabrication by rotary screen printing. See experimental details for printing speed and other parameters of each separate process step. (b) Picture of VTT's ROKO line located at Oulu, Finland.

MO thin films with high quality [35]. Typically, the most common solvent is 2-ME. However, this volatile solvent has high toxicity and, thus, is not appropriate for upscaling to pilot-scale R2R environments. Greener solvents are preferable such as water and ethanol, but these suffer from smaller polymeric chain and high evaporation rate, respectively. These features lead to more defects and non-uniformity in the printed films. Another solvent with promising characteristics is 1-MP, having a low boiling point ($\leqslant$130 °C—compatible with low-cost flexible substrates), a larger polymeric chain like 2-ME, low evaporation rate, and most importantly lower toxicity than 2-ME, thus being suitable for large-area manufacturing. In this study, we explore the role of 1-MP to synthetize and produce ZTO thin films with solution-processing techniques ranging from spin-coating to high-throughput R2R-printing techniques.

2.1. Synthesis and design of ZTO thin films for diodes application

To achieve the optimal synthesis route to produce ZTO (1:1 Zn:Sn-ratio) thin films at low processing temperatures, two methods were considered: conventional sol–gel synthesis and SCS where urea and ammonium nitrate were added as fuel and oxidizer, respectively [25]. Thermogravimetry (TG) and differential scanning calorimetry (DSC) was made on ZTO (1:1) sol–gel and SCS xerogel, as shown in figure 2(a). The DSC analysis of the ZTO sol–gel xerogel show a broad exothermic peak at 103 °C with a mass loss of 27%. This conventional method requires higher temperatures, between 400 °C and 500 °C, to fully convert the ZTO precursors and for degradation of remaining residual mass as observed in the TG data. In comparison, the stoichiometric ZTO SCS xerogel presents two main exothermic peaks during the

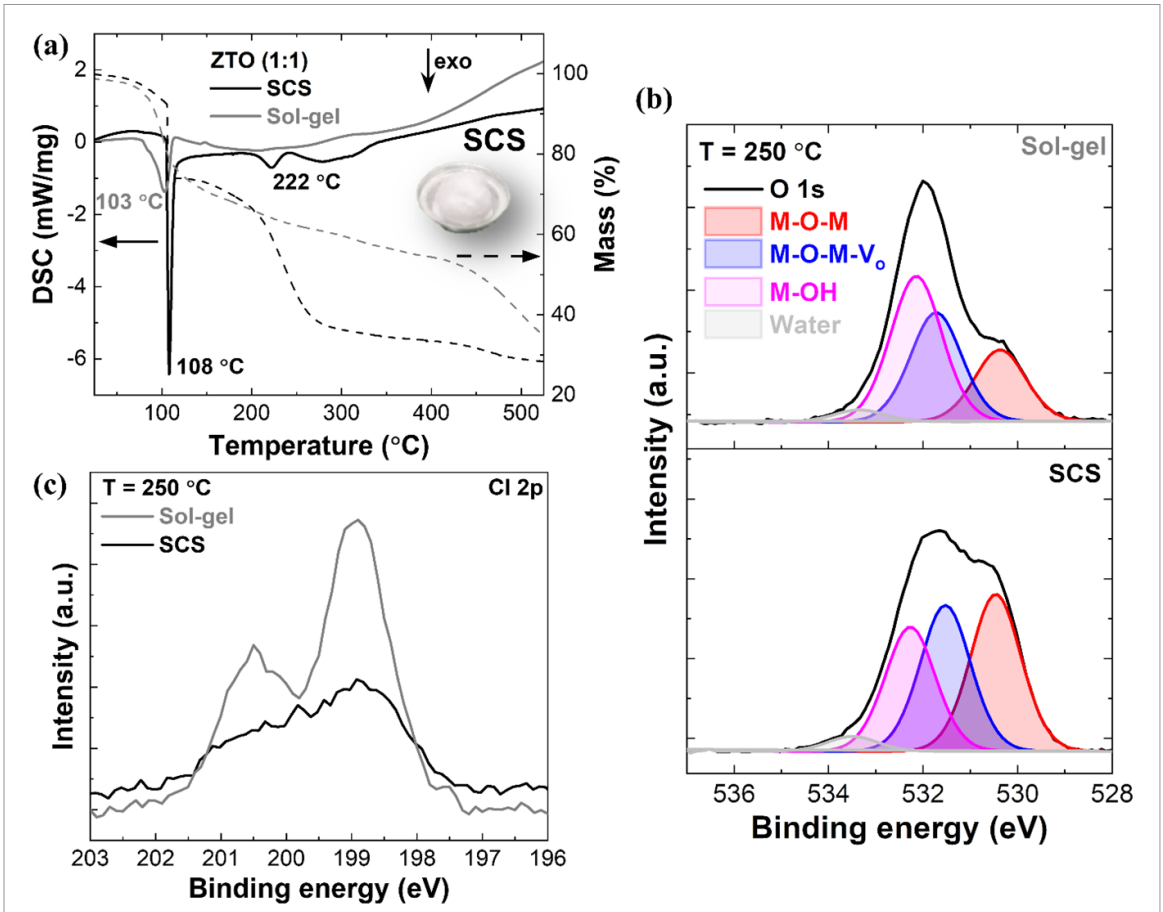

Figure 2. (a) TG-DSC analysis of ZTO (1:1) precursor sol–gel and SCS xerogel. (b) Deconvoluted x-ray photoelectron spectroscopy (XPS) O 1s and (c) Cl 2p emission peaks of the ZTO thin films for different processing conditions: sol–gel and SCS.

combustion reaction process; an intense exothermic peak at 108 °C and a smaller broad exothermic peak at 222 °C, resulting in a mass loss of 26% and 38.7%, respectively. In this case, it is possible to fully convert the ZTO precursors at approximately 250 °C. The main differences between the two methods are related to the absence of an oxidizer (ammonium nitrate) in the tin chloride precursor and the use of urea as fuel to initiate the SCS process leading to high local temperatures at low external temperature [25]. This fuel is highly abundant, presents a high exothermicity at a low ignition temperature (as observed here at 108 °C) and enhanced coordination ability relative to metal nitrate precursors being an ideal candidate [36]. Also, the presence of nitrates is fundamental to promote a good solubility and guarantee homogeneity. In addition, these salt precursors can be decomposed at lower processing temperatures when compared with corresponding acetate and chloride precursors [37]. The images of the solutions in figure S1 in the supporting information clearly show the effect of having a metal nitrate precursor (figure S1 (a)) and the SCS method (figure S1(d)) in the 1-MP-based, upscalable solution synthesis to reach higher homogeneity and solubility once it prevents the hydrolysis of the $SnCl_2$ precursor. Also, the ZTO (1:1) SCS provide higher purity products (white foam-like powder) as depicted in the inset of figure 2(a) at low processing temperatures when compared with the sol–gel method. The ZTO SCS solution in 1-MP is stable, as it does not present any precipitation after one and half years under a controlled environment (figure S2 in the supporting information).

To further study the stoichiometry and the M–O–M bonding of the ZTO thin films annealed at 250 °C produced by the two synthesis methods, XPS measurements were performed, as depicted in figures 2(b), (c), and S3 in the supporting information. Figure 2(b) shows the oxygen main peak (O 1s), which was deconvoluted into four component peaks for the two approaches (see table S2 in the supporting information). These are assigned to oxygen in an oxide lattice (M–O–M), oxygen in vicinity to oxygen vacancies (M–O–M–V_o), hydroxyl (M–OH), and water adsorption at the surface, respectively [38, 39]. When the SCS method is used, the M–O–M bonding of ZTO is enhanced in comparison with the sol–gel approach and the M–OH peak is reduced. In all conditions the tin (Sn $3d_{5/2}$) and the zinc (Zn $2p_{3/2}$) presented peaks with a binding energy at 486.7 ± 0.1 eV and 1022.2 ± 0.1 eV, respectively (see figure S3 in the supporting information). In relation

to Zn:Sn theoretical stoichiometric value (1), Zn:Sn-ratio of 1.59 and 1.26 was achieved for the sol–gel and combustion methods, respectively. The pronounced difference from the theoretical value observed for the ZTO sol–gel is due to two main reasons: the presence of tin hydroxide and unconverted tin chloride. From the appearance of the as-prepared, unfiltered solutions it can be seen that both the tin chloride (figure S1 (b)) and the sol–gel ZTO (figure S1(c)) solutions are not totally transparent due to the formation of tin hydroxides. This leads to ZTO thin films with lower Sn quantity as some of it is lost in the filtration step performed prior to the deposition. Figure 2(c) shows that the Cl 2p peak is more pronounced in the ZTO sol–gel when compared with the SCS being 2.3 times larger (atomic concentration percentage Cl sol–gel/SCS ratio). The residual tin chloride can be converted to tin oxide only if higher annealing temperatures are applied, which is correlated with the results attained in the TG-DSC measurements [40].

To complement the ink and the thin-film characterizations, spin-coated ZTO diodes were produced for the different synthesis methods to determine their electrical performance. To ensure the compatibility in upscaling the fabrication process to pilot-scale R2R environments, the electrode materials need to be patternable using R2R methods. In the vertical ZTO diodes, indium tin oxide (ITO) was used as the bottom (ohmic) electrode as it could be patterned using a R2R-printed ITO etching paste [41]. As the top Schottky contact, conductive polymer poly (3,4-ethylenedioxythiophene):poly(styrenesulfonate) (PEDOT:PSS) was selected as the initial trials performed using printed Ag contacts showed unstable switching characteristics, likely due to Ag ion migration in the oxide layer [42]. Figure 3(a) depicts *I–V* characteristics of the spin-coated vertical ITO/ZTO/PEDOT:PSS-diodes with a sweep from negative to positive voltages and back with stable diode characteristics.

The current rectification ratio is $\sim 10^2$ and $\sim 10^3$ for the sol–gel and SCS ZTO diodes, respectively. The rectification of the ZTO diodes can be explained based on the junction properties of a device structure ITO/ZnO/PEDOT:PSS that bears resemblance to the ITO/ZTO/PEDOT:PSS of this work, since ZTO has a similar or higher band gap as ZnO [43, 44]. The contact ZnO/PEDOT:PSS has been characterized as Schottky type, with an electron injection barrier of 0.8 eV [45]. The ITO/ZnO junction is ohmic [46]. The ideality factor (n), hysteresis (V_{Hyst}) and threshold voltage (V_{T}) are smaller for the ZTO SCS diodes ($n = 5.07 \pm 0.47$; $V_{\mathrm{Hyst}} = 0.17 \pm 0.03$ V; $V_{\mathrm{T}} = 1.49 \pm 0.04$ V) than for the sol–gel diodes ($n = 7.76 \pm 0.44$; $V_{\mathrm{Hyst}} = 0.22 \pm 0.01$ V; $V_{\mathrm{T}} = 1.60 \pm 0.02$ V) due to the enhanced elimination of residual groups that can act as charge traps, such as organics, metal hydroxides and tin chlorides. However, these ideality

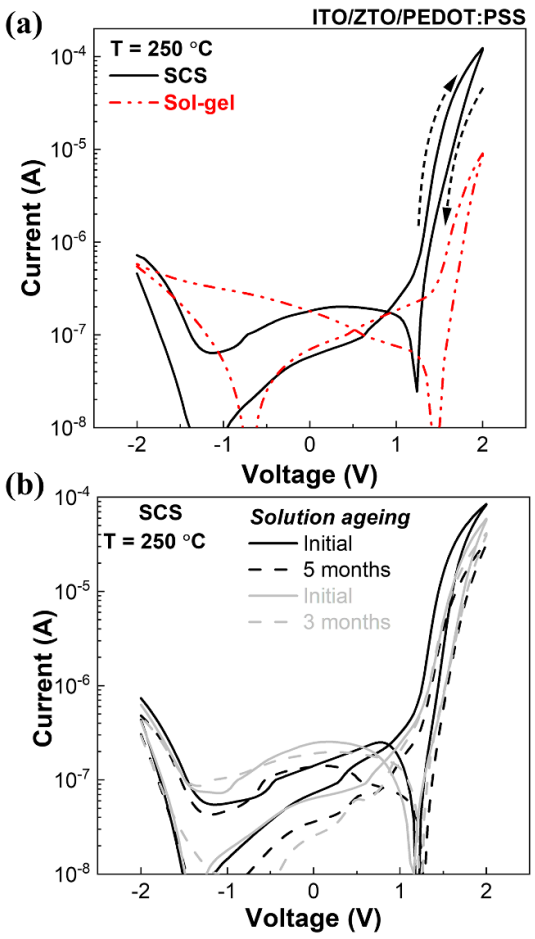

Figure 3. (a) Current–voltage characteristics shown in semi-log plot measured for a representative ITO/ZTO/PEDOT:PSS Schottky diode processed by sol–gel and SCS method using spin coating. (b) Solution ageing effect on ITO/ZTO/PEDOT:PSS diodes produced using the SCS route after 3 and 5 months.

factors are high compared to the typical range expected from a Schottky junction (between 1 and 2). This can be explained by the high density of defects in solution-based ZTO films (compared to physical vapour deposition (PVD) and thermal methods) which act as interface states and recombination centres [47]. In this respect, the ideality factor illustrates the improved film quality when using SCS compared to sol–gel. A total of 16 devices were measured for the sol–gel and SCS ZTO routes, where the SCS route showed a high reproducibility. The sol–gel route diodes presented fewer working devices (figure S4 in the supporting information) once 12 of them did not present any modulation (open-circuit). These electrical results are in accordance with the earlier results (figure 2) from the ink (TG-DSC analysis) and thin film (XPS analysis) characterization suggesting that the ZTO films obtained through the SCS route are superior to those obtained through the sol–gel route.

We now focus on the ZTO diodes obtained from the SCS route. To determine the stability and use-life of the ZTO SCS ink, tests were performed by producing ZTO diodes with inks aged for 3 and 5 months,

as shown in figure 3(b). When the ZTO SCS inks are stored in fridge temperature, no significant changes in the diode performance were noticed when comparing the devices produced with aged inks with the devices produced using the fresh inks (initial), which further supports the reliability of the SCS ink.

2.2. Low temperature approach with IR curing

To reach even lower annealing temperatures and shorter processing times which would be needed to be able to utilize the SCS ZTO inks on low-cost flexible substrates in pilot-scale R2R environments, IR annealing was incorporated to the process and compared with the typical thermal annealing done at 250 °C for 30 min. Taking that into account, the ZTO SCS thin films were dried for 5 min on a hotplate at 140 °C followed by an IR annealing for 7 min in air environment. This IR curing leads to the formation of high-quality ZTO thin films as it promotes the M–O–M network formation [31, 34]. The ZTO SCS thin films were characterized by attenuated total reflection Fourier transform infrared spectroscopy (ATR-FTIR) to assess the solvent removal and ink conversion, as depicted in figure 4(a). For both high temperature annealing (250 °C) and IR curing the ZTO thin films did not afterwards present C–H and OH bonds related to organic precursors in the film which confirms the elimination of all residual organics [34]. The absorption peaks presented at 615 and 582 cm^{-1} are attributed to the Sn–O and Zn–O chemical bonds, respectively [48–50]. Also, the bonding between Zn–O is in the range of 400–700 cm^{-1}. Both films exhibited an amorphous nature with the absence of any diffraction peaks and high transparency (⩾85%) (figures S5 and S6 in the supporting information).

The ZTO diodes annealed by IR presented a similar electrical performance compared to the reference devices annealed at 250 °C, as shown in figure 4(b). The same rectification ratio ($\sim 10^3$) was achieved for both conditions, however, smaller threshold voltage of 1.40 ± 0.06 V was reached with the ZTO diodes annealed by IR. Besides that, these devices present a better ideality factor (5.71 ± 0.50), when compared with the sol–gel ZTO diodes annealed at higher temperature. The hysteresis curves cross each other and is more evident in the devices annealed by IR (V_{Hyst} = 0.29 ± 0.03 V) related to charge traps. These ZTO devices annealed by IR present a promising reproducibility and low threshold voltage variability (figure S7 in the supporting information).

2.3. Lab-scale printing and large-scale manufacturing of the ZTO diodes

After confirming that these ZTO devices can be fabricated at low processing temperatures and that they can be produced in a short processing time using IR annealing, lab-scale printing tests were performed before implementation in the pilot-scale R2R environment. First, ZTO thin films were printed by lab-scale flexographic printing to flexible ITO-covered PET substrates. To assure good adhesion of the ZTO layer, the substrates were exposed to 1 min O_2 plasma before printing. Figure 5(a) depicts the printing of ZTO layers with different ink concentrations (0.6, 1.0 and 1.5 M) using a printing speed of 50 m min^{-1} and an anilox transfer volume of 4 ml m^{-2}. A visible increment of the printed semiconductor layer thickness is observed when the concentration is increased. This is directly proportional to the ink's viscosity as shown in figure S8 in the supporting information. Furthermore, the ZTO SCS ink formulation presents higher thickness when compared to the sol–gel ink formulation (SCS composition contains urea that also acts as an additive to increase the viscosity). This helps to print thicker layers that are needed for vertical diodes to avoid short-circuited devices. However, in figure 5(a) it can be observed that for the highest concentration of 1.5 M, the layer is not uniform having more defects and presenting the coffee-ring effect leading to thicker edges. Therefore, to sustain adequate thickness and a good uniformity for the ZTO diode production in the pilot-scale R2R-process, a concentration of 1.0 M was selected for the further work.

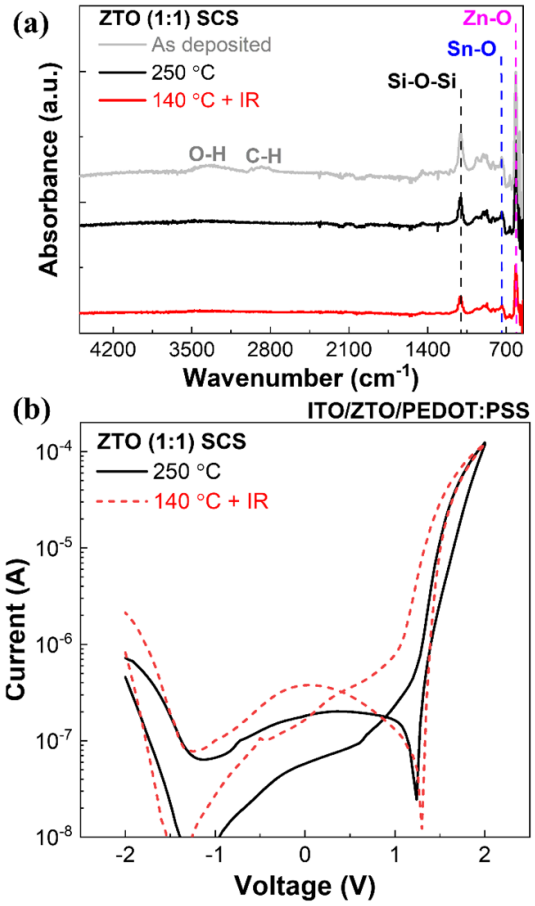

Figure 4. (a) FTIR spectra of ZTO (1:1) SCS thin films. (b) Spin-coated ZTO diode current–voltage characteristics for different annealing conditions with IR curing and thermal annealing at 250 °C.

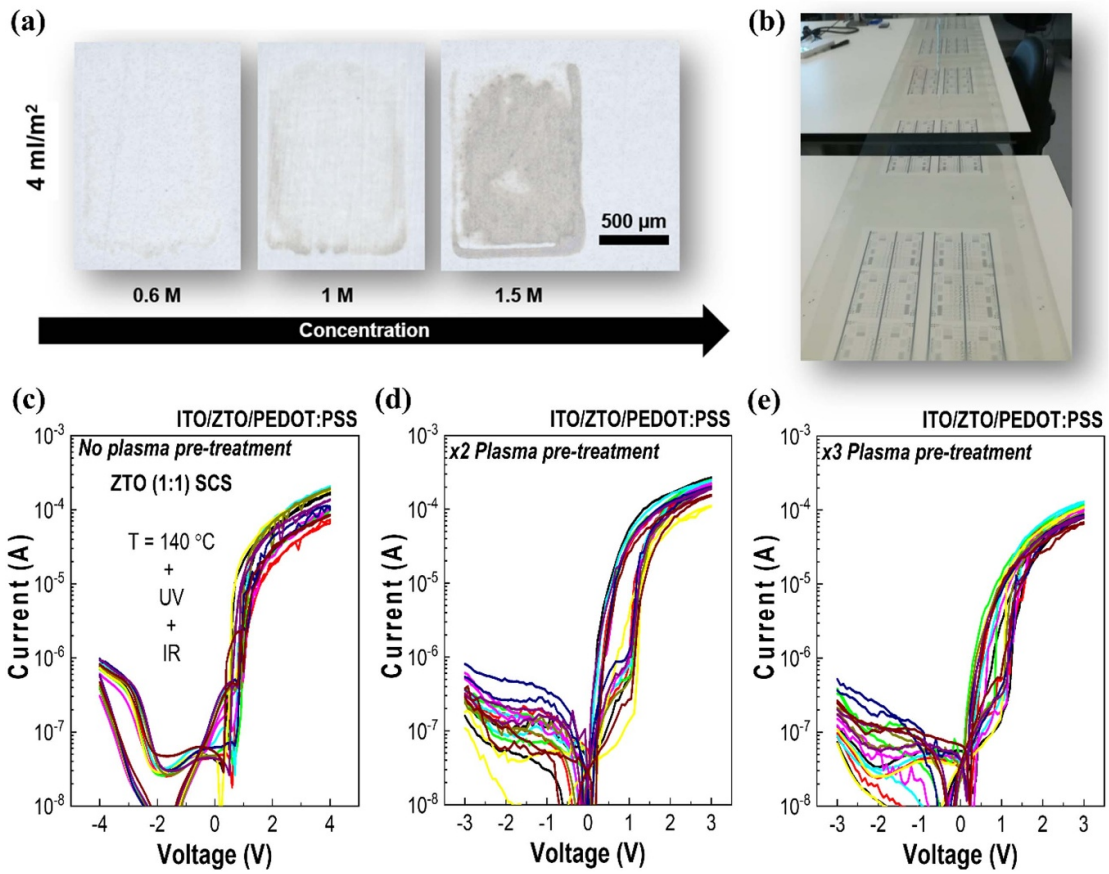

Figure 5. (a) Flexographic printing patterns of ZTO (1:1) SCS using different ink concentration for a printing speed of 50 m min^{-1}. (b) Picture of the ZTO diodes printed in the pilot-scale R2R-printing line. Current–voltage characteristics measured of ZTO diodes produced using 1.0 M SCS ink and three successive ZTO layers under different conditions using pilot-scale R2R processing: (c) no plasma pre-treatment; (d) 2× plasma pre-treatment performed before the second and third ZTO layer; and (e) plasma pre-treatment before all ZTO layers.

After the pre-trials done using the lab-scale flexography printing, the process was transferred to pilot-scale R2R-printing line (ROKO at VTT, figures 1(b) and 5(b)). Several optimization cycles were undertaken to optimize the printing parameters of the ZTO inks (anilox volume: 5 ml m^{-2}; printing speed: 10 m min^{-1}; three successive ZTO layers) and the curing parameters (140 °C ovens followed by two UV units and final curing using IR ovens) in the R2R pilot-line. To improve the quality of the printed ZTO layers and the overall performance of the ZTO diodes, a plasma treatment was performed to the substrate containing the R2R-patterned ITO layers as well as in between the printed ZTO to assure a good adhesion and avoid the poor quality of the overprinted layers (figure S9 in the supporting information). Figures 5(c)–(e) shows the electrical performance of the R2R-processed ZTO diodes printed with and without the plasma treatment before the deposition of each ZTO layer. For all conditions, at least ten devices were measured, showing diode characteristics with a good reproducibility and low variability. Especially, the devices with 2× plasma treatment (first layer without and 2nd and 3rd layer with plasma) in figure 5(c) show ∼1 V turn-on voltage, $\sim 10^3$ rectification ratio and small, consistent hysteresis loop. The comparison of these results to those obtained with spin-coated ZTO (figures 3(a), (b) and S4(b)) indicates that it is possible to upscale the ZTO inks from the lab-scale to pilot-scale R2R-production, while maintaining a similar level of electrical performance. Although a thorough roll-level statistical analysis of the R2R printed diodes was not performed, the promising reproducibility obtained for the devices clearly demonstrates the printability of the upscaled ZTO ink at a pilot scale. To our knowledge, this is the first demonstration of such R2R MO diodes in a pilot-scale R2R environment, especially using inks consisting less-toxic solvents (1-MP instead of 2-ME). In future work, efforts in device size scaling and passivation need to assure their compatibility with various flexible electronics applications, such as a rectifier for the anti-counterfeit label combining electrochromic display and near field communication (NFC) reading [51].

3. Conclusions

In summary, we reported the relevance of SCS in the formation of ZTO (1:1) thin films using a greener

solvent (1-MP) and the use of low processing temperatures (140 °C). This was achieved by the combination with IR annealing in a short processing time and demonstrates upscaling from lab-scale to pilot-scale R2R environments. For the first time, fully pilot-scale R2R-processed ZTO diodes were produced with R2R-etched ITO bottom electrode and printed PEDOT:PSS top electrode. The ZTO diodes exhibit promising electrical features, such as $\sim 10^3$ rectification ratio, promising reproducibility, low threshold voltage deviation, and low operating voltage. The achieved results take the processability of MOs a step closer to the production lines used in the printing industry. Such MO semiconductor devices could be of use in various large-volume flexible electronics applications and complement the new era of sustainable hybrid electronics.

4. Experimental section

4.1. Precursor solution synthesis and characterization

Sol–gel ink: Zinc nitrate precursor ($Zn(NO_3)_2 \cdot 6H_2O$, Sigma-Aldrich, ⩾99.0%) was dissolved in 1-methoxy-2-propanol (1-MP, $C_4H_{10}O_2$, Carl ROTH, ⩾99.0%) to yield the zinc oxide precursor solution. For the synthesis of the Zn precursor solution, stirring at 65 °C was performed to improve the dissolution. Afterwards, tin chloride precursor ($SnCl_2 \cdot 2H_2O$, Sigma-Aldrich, ⩾98.0%) was dissolved in 1-MP. As soon as the tin chloride solution was clear, the two solutions (zinc and tin precursors) were mixed in 1:1 Zn:Sn molar ratio and magnetically stirred (430 rpm) for at least 12 h at room temperature in air environment.

Combustion (SCS) ink: The zinc nitrate precursor and ammonium nitrate (NH_4NO_3, Carl ROTH, ⩾98.0%) were added sequentially to 1-MP. To facilitate the precursor dissolution, the solution was stirred at 65 °C. Afterwards, urea ($CO(NH_2)_2$, Sigma-Aldrich, ⩾99.0%) was dissolved into the solution. To guarantee the redox stoichiometry of the combustion reaction, a molar ratio between urea and zinc nitrate of (5/3):1 was used. The oxidizing agent, ammonium nitrate, was added to act as an oxidizer for the tin chloride with a molar proportion of 2:1 between ammonium nitrate and $SnCl_2$. For the ammonium nitrate precursor, the urea molar proportion was 1:(2/3). To finalize the synthesis, the tin chloride ink was added to the solution (mixture of zinc nitrate, ammonium nitrate and urea) as described previously for the sol–gel ink to yield Zn:Sn molar ratio of 1:1. All precursor solutions were filtrated through 0.45 μm pore size hydrophilic filters before use.

Different solute concentrations (0.6, 1, 1.2, 1.5 M) were tested to assure good quality of the spin-coated and printed layers. The viscosity measurements of the ZTO inks were performed using a BROOKFIELD Cap 2000+ (Brookfield Engineering Laboratories, Inc., Middleboro, MA, USA) with a Cap01 spindle at 25 °C and at 500 rpm speed.

TG-DSC measurements (Netzsch, TG-DSC—STA 449 F3 Jupiter) were performed for the ZTO (1:1) inks (sol–gel and SCS) under air atmosphere up to 500 °C with a 10 °C min^{-1} heating rate in an aluminium crucible. The samples were prepared by drying 10 ml of ZTO precursor solutions on a hotplate at 65 °C with magnetic stirring at 300 rpm until a viscous gel was obtained.

4.2. ZTO film deposition and characterization

Prior to deposition, rigid substrates (p-type silicon wafer, glass and commercial glass with ITO with an area of 2.5 × 2.5 cm^2) were cleaned as described in a previous work [34]. To improve the wettability of the ZTO inks, a UV/ozone surface activation step was performed in a PSD-UV Novascan system for 10 min at a lamp distance of 5 cm. To produce the ZTO (1:1) thin films, sol–gel and SCS precursor solutions were deposited by spin-coating with a concentration of 0.6 M for 35 s at 2000 rpm (Laurell Technologies). An immediate thermal annealing at 140 °C for 5 min was performed to dry the samples being followed by either an IR curing (Infrared IC heater, T-962, Reflow Oven) for 7 min or annealing at 250 °C on a hotplate for 30 min. A second ZTO layer was deposited using the same conditions as the previous one after performing a UV/ozone surface treatment to improve the adhesion between the layers.

Flexible substrates (polyimide and PET with ITO) were cleaned with ethanol in an ultra-sonic bath and dried with N_2. Afterwards, an O_2 plasma treatment (Diener Plasma Surface Technology) was performed for 1 min to improve wettability. To investigate the printability of the ZTO inks, flexographic printing of the ZTO layer with ink a concentration of 1.0 M was performed using RK Flexiproof 100 table-top printing machine. The printing was tested at 50 m min^{-1} printing speed using anilox rolls with different transfer volumes: 3 ml m^{-2} (400 lines cm^{-1}), and 4 ml m^{-2} (320 lines cm^{-1}) while assuring a proper ink transfer from patterned flexo stamp to the substrate through low nip pressure (kiss pressure). After printing, all the samples were dried at 140 °C on a hotplate in air for 10 min and investigated using an optical microscope. All the lab-scale deposition and drying tests of the ZTO inks were performed in controlled ambient conditions where the relative humidity and temperature varied between 40%–44% and 23.5 °C–24.2 °C, respectively.

The crystal structure and the absorption peaks of the constituents of the ZTO thin films deposited on Si substrates were assessed by glancing angle x-ray diffraction and ATR-FTIR, respectively, as described in a previous work [34]. XPS was done with a Kratos Axis Supra spectrometer using monochromatic Al Kα radiation. The detail scans were recorded with a

constant pass energy of 10 eV. Data analysis was conducted with CasaXPS version 2.3.19PR1.0.

4.3. Lab-scale ZTO diode production and characterization

Vertical ZTO Schottky diodes were prepared using the sol–gel and SCS ZTO inks on commercial glass/ITO substrates as mentioned above (ITO bottom electrode). Afterwards, PEDOT doped with PSS (PEDOT:PSS, Sigma-Aldrich, 5.0 wt.%, conductive screen printable ink) was deposited as the top electrode to provide Schottky contact by screen printing and annealed on a hotplate at 130 °C for 3 min. The active area of these ZTO devices was 1000 μm × 1000 μm.

4.4. Pilot-scale R2R-processed ZTO diode fabrication and characterization

The up-scaled ZTO diodes were processed onto ITO bottom electrodes that were patterned using R2R-printed ITO etching paste [41] on flexible PET substrates in the ROKO pilot-line at VTT facility (factory scale-up) in Oulu. Then, ZTO SCS precursor ink with 1 M concentration was printed on top of the bottom electrode lines with printing direction perpendicular to the ITO bottom electrode lines as three successive ZTO layers with overlay registration. The printing was optimized for homogeneous ZTO layers using a printing speed of 10 m min^{-1} and anilox rolls with 5 ml m^{-2} transfer volume (320 lines cm^{-1}). Prior to the deposition of the ZTO thin films and between the successive ZTO layers, in-line plasma treatment (Ar/N_2, 550 W) was performed to improve the adhesion of these layers to the ITO electrode and improve the printing quality of the overlaying layers. After the printing of each ZTO layer, the PET/ITO web with the printed ZTO layer was dried with an in-line speed of 10 m min^{-1} using in-line drying oven at 140 °C (four ovens with total ∼4 m length leading to ∼24 s total drying time) and two in-line 365 nm UV drying units (160 W cm^{-1} at 55% and 80% power with total ∼0.25 m length leading to ∼1.5 s curing time). As mentioned earlier, this process was repeated two more times to have total 3× layer of ZTO (rewind the printing roll in the ROKO pilot-line) and then, to finalize the curing of the active layer, an IR irradiation (3 × 1 kW IR lamps with 9 s treatment time with 10× cycles leading to total 90 s annealing time) was applied with a printing inline speed of 2 m min^{-1}. The thickness of the cured (3×) ZTO layer was approximately 60–80 nm when measured using a stylus profilometer (Veeco Dektak). To finalize the vertical ZTO diodes, PEDOT:PSS (AFGA Orgacon EL-P5015) top electrode was deposited by R2R rotary screen (215 meshes inch^{-1}) printing with a printing speed of 2 m min^{-1} (after rewind the printing roll in the ROKO pilot-line) and dried at 140 °C (four ovens with total drying time of ∼2 min). The active area (i.e. overlap between ITO and PEDOT:PSS electrodes) of the ZTO devices was ∼100 μm × ∼100 μm.

The electrical characterization of the lab-scale and R2R-processed ZTO Schottky-diodes was performed in dark environment using a semiconductor parameter analyser (Keysight 4200SCS) and probe station (Janis ST-500). Back and forth current–voltage ($I-V$) characteristics were recorded by sweeping the voltage in 0.05 V steps using a 0.05 s step time. To calculate the ideality factor the method proposed by Werner *et al* was applied, using the increasing sweep in the forward polarity [52].

Data availability statement

All data that support the findings of this study are included within the article (and any supplementary files).

Acknowledgments

This work is funded in part by National Funds through FCT—Fundação para a Ciência e Tecnologia, I P, under the scope of the project UIDB/50025/2020. E Carlos acknowledges the postdoctoral grant (Grant No. 951774) from the project FOXES. VTT's and FCT's work was funded in part by European Institute of Innovation and Technology (EIT RawMaterials, Horizon 2020) Supersmart, Scale-Up of Printed Electronics, Grant Agreement 17161. Part of the facilities used at VTT were provided by the Academy of Finland Research Infrastructure Printed Intelligence Infrastructure (PII-FIRI, Grant No. 32020). E Fortunato acknowledges the ERC AdG Grant 787410 from the project DIGISMART. We acknowledge to the project SYNERGY H2020-WIDESPREAD-2020-5, CSA, proposal No. 952169. M Alexandre is thanked for technical assistance to make the R2R schematic. P Hakkarainen, A Pesonen, and Hannu Sääskilahti from VTT are thanked for technical assistance and operation of the roll-to-roll pilot line ROKO.

ORCID iDs

Emanuel Carlos https://orcid.org/0000-0002-5956-5757
Rita Branquinho https://orcid.org/0000-0001-9771-8366
Jaakko Leppäniemi https://orcid.org/0000-0001-5865-0135
Jonas Deuermeier https://orcid.org/0000-0002-2764-3124
Ari Alastalo https://orcid.org/0000-0003-4999-6956

Liisa Hakola https://orcid.org/0000-0002-8394-6277
Elvira Fortunato https://orcid.org/0000-0002-4202-7047
Rodrigo Martins https://orcid.org/0000-0002-1997-7669

References

[1] Wang Y, Lin Y, Zhong R Y and Xu X 2019 IoT-enabled cloud-based additive manufacturing platform to support rapid product development *Int. J. Prod. Res.* **57** 3975–91
[2] Eid A, He X, Bahr R, Lin T, Cui Y, Adeyeye A, Tehrani B and Tentzeris M M 2020 Inkjet-/3D-/4D-printed perpetual electronics and modules: RF and mm-wave devices for 5G+, IoT, smart agriculture, and smart cities applications *IEEE Microwave Mag.* **21** 87–103
[3] Biggs J, Myers J, Kufel J, Ozer E, Craske S, Sou A, Ramsdale C, Williamson K, Price R and White S 2021 A natively flexible 32-bit Arm microprocessor *Nature* **595** 532–6
[4] Wu W 2017 Inorganic nanomaterials for printed electronics: a review *Nanoscale* **9** 7342–72
[5] Khan Y, Thielens A, Muin S, Ting J, Baumbauer C and Arias A C 2020 A new frontier of printed electronics: flexible hybrid electronics *Adv. Mater.* **32** 1905279
[6] Coelho J, Kremer M P, Pinilla S and Nicolosi V 2020 An outlook on printed microsupercapacitors: technology status, remaining challenges, and opportunities *Curr. Opin. Electrochem.* **21** 69–75
[7] Ramon E, Sowade E, Martínez-Domingo C, Mitra K Y, Alcalde A, Baumann R R and Carrabina J 2021 Large-scale fabrication of all-inkjet-printed resistors and WORM memories on flexible polymer films with high yield and stability *Flex. Print. Electron.* **6** 015003
[8] Chu Y, Qian C, Chahal P and Cao C 2019 Printed diodes: materials processing, fabrication, and applications *Adv. Sci.* **6** 1801653
[9] Carlos E, Leppäniemi J, Sneck A, Alastalo A, Deuermeier J, Branquinho R, Martins R and Fortunato E 2020 Printed, highly stable metal oxide thin-film transistors with ultra-thin high-κ oxide dielectric *Adv. Electron. Mater.* **6** 1901071
[10] Carlos E, Branquinho R, Martins R, Kiazadeh A and Fortunato E 2021 Recent progress in solution-based metal oxide resistive switching devices *Adv. Mater.* **33** 2004328
[11] Choudhary I and Deepak 2017 Flexible substrate compatible solution processed P-N heterojunction diodes with indium-gallium-zinc oxide and copper oxide *Mater. Sci. Eng.* B **218** 64–73
[12] Semple J, Rossbauer S, Burgess C H, Zhao K, Jagadamma L K, Amassian A, McLachlan M A and Anthopoulos T D 2016 Radio frequency coplanar ZnO Schottky nanodiodes processed from solution on plastic substrates *Small* **12** 1993–2000
[13] Vieira D H, da Silva Ozório M, Nogueira G L, Fugikawa-Santos L and Alves N 2021 UV-photocurrent response of zinc oxide based devices: application to ZnO/PEDOT:PSS hydrid Schottky diodes *Mater. Sci. Semicond. Process.* **121** 105339
[14] Georgiadou D G *et al* 2020 100 GHz zinc oxide Schottky diodes processed from solution on a wafer scale *Nat. Electron.* **3** 718–25
[15] Garlapati S K, Divya M, Breitung B, Kruk R, Hahn H and Dasgupta S 2018 Printed electronics based on inorganic semiconductors: from processes and materials to devices *Adv. Mater.* **30** 1707600
[16] Carlos E, Branquinho R, Martins R and Fortunato E 2021 New challenges of printed high-κ oxide dielectrics *Solid State Electron.* **183** 108044
[17] Shao F and Wan Q 2019 Recent progress on jet printing of oxide-based thin film transistors *J. Phys. D: Appl. Phys.* **52** 143002
[18] Leppäniemi J, Huttunen O-H H, Majumdar H and Alastalo A 2015 Flexography-printed in $2O_3$ semiconductor layers for high-mobility thin-film transistors on flexible plastic substrate *Adv. Mater.* **27** 7168–75
[19] Leppäniemi J, Sneck A, Kusaka Y, Fukuda N and Alastalo A 2019 Reverse-offset printing of metal-nitrate-based metal oxide semiconductor ink for flexible TFTs *Adv. Electron. Mater.* **5** 1900272
[20] Grau G, Cen J, Kang H, Kitsomboonloha R, Scheideler W J and Subramanian V 2016 Gravure-printed electronics: recent progress in tooling development, understanding of printing physics, and realization of printed devices *Flex. Print. Electron.* **1** 1–23
[21] Hösel M, Søndergaard R R, Jørgensen M and Krebs F C 2013 Fast inline roll-to-roll printing for indium-tin-oxide-free polymer solar cells using automatic registration *Energy Technol.* **1** 102–7
[22] Park H, Kang H, Lee Y, Park Y, Noh J and Cho G 2012 Fully roll-to-roll gravure printed rectenna on plastic foils for wireless power transmission at 13.56 MHz *Nanotechnology* **23** 344006
[23] Kang H, Park H, Park Y, Jung M, Kim B C, Wallace G and Cho G 2015 Fully roll-to-roll gravure printable wireless (13.56 MHz) sensor-signage tags for smart packaging *Sci. Rep.* **4** 5387
[24] Carlos E, Branquinho R, Barquinha P, Martins R and Fortunato E 2021 New strategies toward high-performance and low-temperature processing of solution-based metal oxide TFTs *Chemical Solution Synthesis for Materials Design and Thin Film Device Applications* (Elsevier) pp 585–621
[25] Kim M-G, Kanatzidis M G, Facchetti A and Marks T J 2011 Low-temperature fabrication of high-performance metal oxide thin-film electronics via combustion processing *Nat. Mater.* **10** 382–8
[26] Carlos E, Martins R, Fortunato E and Branquinho R 2020 Solution combustion synthesis: towards a sustainable approach for metal oxides *Chem. Eur. J.* **26** 9099–125
[27] Yarali E, Koutsiaki C, Faber H, Tetzner K, Yengel E, Patsalas P, Kalfagiannis N, Koutsogeorgis D C and Anthopoulos T D 2019 Recent progress in photonic processing of metal-oxide transistors *Adv. Funct. Mater.* **30** 1906022
[28] Carlos E, Dellis S, Kalfagiannis N, Koutsokeras L, Koutsogeorgis D C, Branquinho R, Martins R and Fortunato E 2020 Laser induced ultrafast combustion synthesis of solution-based AlO_x for thin film transistors *J. Mater. Chem.* C **8** 6176–84
[29] Kim Y-H, Heo J-S, Kim T-H, Park S, Yoon M-H, Kim J, Oh M S, Yi G-R, Noh Y-Y and Park S K 2012 Flexible metal-oxide devices made by room-temperature photochemical activation of sol–gel films *Nature* **489** 128–32
[30] Benwadih M, Coppard R, Bonrad K, Klyszcz A and Vuillaume D 2016 High mobility flexible amorphous IGZO thin-film transistors with a low thermal budget ultra-violet pulsed light process *ACS Appl. Mater. Interfaces* **8** 34513–9
[31] Moon C-J and Kim H-S 2019 Intense pulsed light annealing process of indium–gallium–zinc–oxide semiconductors via flash white light combined with deep-UV and near-infrared drying for high-performance thin-film transistors *ACS Appl. Mater. Interfaces* **11** 13380–8
[32] Tetzner K, Lin Y-H, Regoutz A, Seitkhan A, Payne D J and Anthopoulos T D 2017 Sub-second photonic processing of solution-deposited single layer and heterojunction metal oxide thin-film transistors using a high-power xenon flash lamp *J. Mater. Chem.* C **5** 11724–32
[33] Leppäniemi J, Eiroma K, Majumdar H and Alastalo A 2017 Far-UV annealed inkjet-printed in $2O_3$ semiconductor layers for thin-film transistors on a flexible polyethylene naphthalate substrate *ACS Appl. Mater. Interfaces* **9** 8774–82
[34] Carlos E, Branquinho R, Kiazadeh A, Martins J, Barquinha P, Martins R and Fortunato E 2017 Boosting electrical performance of high-κ nanomultilayer dielectrics and

electronic devices by combining solution combustion synthesis and UV irradiation *ACS Appl. Mater. Interfaces* **9** 40428–37
[35] Lim K-H, Lee J, Huh J-E, Park J, Lee J-H, Lee S-E and Kim Y S 2017 A systematic study on effects of precursors and solvents for optimization of solution-processed oxide semiconductor thin-film transistors *J. Mater. Chem.* C **5** 7768–76
[36] Zhang J, Guo Q, Liu Y and Cheng Y 2012 Preparation and characterization of Fe_2O_3/Al_2O_3 using the solution combustion approach for chemical looping combustion *Ind. Eng. Chem. Res.* **51** 12773–81
[37] Kim S J, Yoon S and Kim H J 2014 Review of solution-processed oxide thin-film transistors *Jpn. J. Appl. Phys.* **53** 02BA02
[38] Lee Y G and Choi W-S 2014 Electrohydrodynamic jet-printed zinc–tin oxide TFTs and their bias stability *ACS Appl. Mater. Interfaces* **6** 11167–72
[39] Moulder J F, Stickle W F, Sobol P E and Bomben K D 1992 *Handbook of X-Ray Photoelectron Spectroscopy* (Waltham, MN: Perkin-Elmer Corporation)
[40] Rohnacher V *et al* 2021 Analytical study of solution-processed tin oxide as electron transport layer in printed perovskite solar cells *Adv. Mater. Technol.* **6** 2000282
[41] Kopola P *et al* 2011 Gravure printed flexible organic photovoltaic modules *Sol. Energy Mater. Sol. Cells* **95** 1344–7
[42] Carlos E, Branquinho R, Martins R, Kiazadeh A and Fortunato E 2021 Recent progress in solution-based metal oxide resistive switching devices *Adv. Mater.* **33** 2004328
[43] Lindahl J, Keller J, Donzel-Gargand O, Szaniawski P, Edoff M and Törndahl T 2016 Deposition temperature induced conduction band changes in zinc tin oxide buffer layers for $Cu(In,Ga)Se_2$ solar cells *Sol. Energy Mater. Sol. Cells* **144** 684–90
[44] Rovisco A, Branquinho R, Martins J, Oliveira M J, Nunes D, Fortunato E, Martins R and Barquinha P 2018 Seed-layer free zinc tin oxide tailored nanostructures for nanoelectronic applications: effect of chemical parameters *ACS Appl. Nano Mater.* **1** 3986–97
[45] Nagata T, Oh S, Yamashita Y, Yoshikawa H, Hayakawa R, Kobayashi K, Chikyow T and Wakayama Y 2012 Hard x-ray photoelectron spectroscopy study on band alignment at poly(3,4-ethylenedioxythiophene): poly(styrenesulfonate)/ZnO interface *Appl. Phys. Lett.* **101** 173303
[46] Wager J F 2008 Transparent electronics: Schottky barrier and heterojunction considerations *Thin Solid Films* **516** 1755–64
[47] Chan K-Y, Ng Z-N, Au B W-C and Knipp D 2018 Visibly transparent metal oxide diodes prepared by solution processing *Opt. Mater.* **75** 595–600
[48] Narasimman S, Dinesh U, Balakrishnan L, Meher S R, Sivacoumar R and Alex Z C 2017 A comparative study on structural, optical and humidity sensing characteristics of ZnO, SnO_2 and ZnO:SnO_2 nanocomposite *Sens. Lett.* **15** 440–7
[49] Kayani Z N, Iqbal M, Riaz S, Zia R and Naseem S 2015 Fabrication and properties of zinc oxide thin film prepared by sol-gel dip coating method *Mater. Sci. -Poland* **33** 515–20
[50] Kumari R, Sahai A and Goswami N 2015 Effect of nitrogen doping on structural and optical properties of ZnO nanoparticles *Prog. Nat. Sci. Mater. Int.* **25** 300–9
[51] Hakola L, Jansson E, Futsch R, Happonen T, Thenot V, Depres G, Rougier A and Smolander M 2021 Sustainable roll-to-roll manufactured multi-layer smart label *Int. J. Adv. Manuf. Technol.* **117** 2921–34
[52] Werner J H 1988 Schottky barrier and pn-junction I/V plots—small signal evaluation *Appl. Phys.* A **47** 291–300